



# Spherical lithium-rich layered $\text{Li}_{1.13}[\text{Mn}_{0.534}\text{Ni}_{0.233}\text{Co}_{0.233}]_{0.87}\text{O}_2$ with concentration-gradient outer layer as high-performance cathodes for lithium ion batteries

Xiukang Yang, Xianyou Wang\*, Guishan Zou, Liang Hu, Hongbo Shu, Shunyi Yang, Li Liu, Hai Hu, Hao Yuan, Benan Hu, Qiliang Wei, Lanhua Yi

Key Laboratory of Environmentally Friendly Chemistry and Applications of Ministry of Education, School of Chemistry, Xiangtan University, Hunan, Xiangtan 411105, China

## HIGHLIGHTS

- Spherical  $\text{Li}_{1.13}[\text{Mn}_{0.534}\text{Ni}_{0.233}\text{Co}_{0.233}]_{0.87}\text{O}_2$  was synthesized by co-precipitation.
- The material comprised a core encapsulated with concentration-gradient outer layer.
- The concentration of Mn increased gradually within the outer layer of the material.
- The material showed high performance due to its concentration-gradient architecture.

## ARTICLE INFO

### Article history:

Received 13 October 2012

Received in revised form

25 November 2012

Accepted 3 January 2013

Available online 12 January 2013

### Keywords:

Lithium-rich layered materials  
Concentration-gradient outer layer  
Cathode  
Co-precipitation  
Lithium ion batteries

## ABSTRACT

A spherical lithium-rich layered cathode material with an average composition of  $\text{Li}_{1.13}[\text{Mn}_{0.534}\text{Ni}_{0.233}\text{Co}_{0.233}]_{0.87}\text{O}_2$  was successfully synthesized via co-precipitation route. In this material, each particle was consisted of an inner core and a stable concentration-gradient outer layer in which manganese content was gradually increased. The concentration-gradient material showed a typical rhombohedral  $\text{LiNiO}_2$ -like layered structure with the existence of the monoclinic  $\text{Li}_2\text{MnO}_3$ -type integrated component. It can be found from the cross-sectional SEM images that the concentration-gradient particle was quite homogeneous without any apparent gap between the inner core and the concentration-gradient outer layer. Furthermore, according to the EDXS analysis, the concentrations of Mn, Ni, and Co kept almost constant throughout the core, and the concentration of Mn increased gradually within the outer layer of the particle. The lithium-rich layered material can deliver a very high capacity of  $220 \text{ mAh g}^{-1}$ , and the excellent cycle life and improved thermal stability were achieved by the concentration-gradient outer layer. The results here indicate that the lithium-rich layered material with a manganese-rich concentration-gradient outer layer will be a promising cathode material for advanced lithium ion batteries with high capacity, long cycle life, and improved safety.

© 2013 Elsevier B.V. All rights reserved.

## 1. Introduction

Rechargeable lithium ion batteries are key components of portable electronics and play an important role in today's mobile society. To expand the use of lithium ion batteries, for instance as the onboard energy storage for vehicles, the energy density must be increased. Notoriously, the energy density of the current lithium ion technology is limited by the cathode capacity, and thus there is immense interest to develop new cathode materials with higher

capacity or higher operation voltages [1–3]. In this regard, layered  $\text{LiMO}_2$  ( $\text{M} = \text{Mn, Ni, and Co}$ ) have been attached more attention because of their high capacity of over  $200 \text{ mAh g}^{-1}$  when charged to 4.5 V or higher [4–6]. Nevertheless,  $\text{Li}_{1-x}\text{MO}_2$  structures tend to become unstable at high levels of delithiation. The instability is attributed largely to the highly oxidizing nature of tetravalent cobalt and nickel, which results in the loss of oxygen and the migration of the transition metal ions to the lithium-depleted layer [2,7]. A common procedure used to stabilize metal oxide electrode structures is cation or anion substitution with a series of foreign ions [8], such as Al, Mg, Ti, Fe, or F [9–14]. However, the doping by these ions may result in capacity decreases and/or environmental concerns. Another alternative approach to impart structural

\* Corresponding author. Tel.: +86 731 58292060; fax: +86 731 58292061.

E-mail address: [wxianyou@yahoo.com](mailto:wxianyou@yahoo.com) (X. Wang).

stability and improve the electrochemical properties of electrode materials is to use structural units rather than cation or anion substituent. This strategy was adopted at Argonne National Laboratory to stabilize layered LiMO<sub>2</sub> (M = Mn, Ni, and Co) electrodes by integrating a structurally compatible component Li<sub>2</sub>MnO<sub>3</sub> [15,16]. This type of electrode material is considered as a lithium-rich layered material Li<sub>1+x</sub>[M]<sub>1-x</sub>O<sub>2</sub> (M = Mn, Ni, and Co; x > 0), which is also regarded as a nano-dimensional solid solution between Li<sub>2</sub>MnO<sub>3</sub> and LiMO<sub>2</sub> (M = Mn, Ni, and Co) [2]. As such, they are often written in two-component notation as xLi<sub>2</sub>MnO<sub>3</sub>·(1-x)LiMO<sub>2</sub> (M = Mn, Ni, and Co) [17–20]. In this material, the Li<sub>2</sub>MnO<sub>3</sub> component is significant because it can lend structural stability and provide additional high capacity to electrode if electrochemically activated above 4.5 V. The origin has been ascribed to the fact that the electrochemically inert Li<sub>2</sub>MnO<sub>3</sub> would transform into the electrochemically active MnO<sub>2</sub> after both lithium and oxygen are simultaneously extracted from the lattice during the initial charge process, and the resulting MnO<sub>2</sub> could not only participate the following charge–discharge process, but also function as a structural unit to stabilize the host LiMO<sub>2</sub> structure [2]. Even so, the lithium-rich layered cathode material seems to still have cyclic durability and safety problems due to its unstable Co<sup>4+</sup> ion and Ni<sup>4+</sup> ion in a high cut-off voltage when directly contacting with the electrolyte [21,22].

A widely used strategy to overcome these issues is surface modification by coating/wrapping the positive material particles with other media [23–27]. The coatings can prevent the direct contact between active particles and electrolyte, resulting to decrease side reaction and heat generation during the cycling [28]. However, this beneficial effect may be contrasted with an increase of the battery impedance resulting from the insulating nature of the coating media [29]. In addition, the coating layer is so thin and heterogeneous that it could wear off the cathode surface during long-term cycling if it is subjected to continuous HF attack, leading to a slow fading of the capacity during extensive cycling [30]. Therefore, adopting a new strategy to improve the performance of lithium-rich layered cathode material is urgent. It is well known that manganese-enriched cathode materials have excellent cycle life and safety, which are attributed to their stable tetravalent Mn when in contact with the battery electrolyte [31,32]. Previous efforts have attempted to fabricate “core–shell” materials with a core enriched in Ni for high capacity and a shell enriched in Mn for high stability and cycling performance [33,34]. In these “core–shell” materials, the core is protected by the stable manganese-enriched shell when contacting with the electrolyte, thus it could safely operate with no risk of structural disruption during the long charge–discharge process of lithium ion batteries. However, the composition of the transition metals at the interface between the core and shell changes rather sharply, which would cause a different shrinkage ratio during the high-temperature calcinations process. In that case, the interface between the core and shell could act as a barrier to Li<sup>+</sup> diffusion, thereby resulting in poor electrochemical properties of the materials.

In this work, we report a novel concentration-gradient material of low cost, high capacity, long cycle life, and improved thermal as advanced cathodes for lithium ion batteries. A spherical lithium-rich layered material Li<sub>1.13</sub>[Mn<sub>0.534</sub>Ni<sub>0.233</sub>Co<sub>0.233</sub>]<sub>0.87</sub>O<sub>2</sub>, which had an inner core and a stable concentration-gradient outer layer with increased manganese content, was successfully synthesized via co-precipitation method. The concentration of transition metals was changed gradually and continually in the concentration-gradient outer layer, while the concentration of all metal ions was maintained at a constant value in the inner core. The structure, morphology and electrochemical properties of the as-prepared concentration-gradient cathode material were studied

in detail. In addition, a conventional lithium-rich layered material 0.3Li<sub>2</sub>MnO<sub>3</sub>·0.7Li[Mn<sub>1/3</sub>Ni<sub>1/3</sub>Co<sub>1/3</sub>]O<sub>2</sub>, which had the same chemical composition and did not possess concentration gradient of transition metal ions, was also synthesized for comparison.

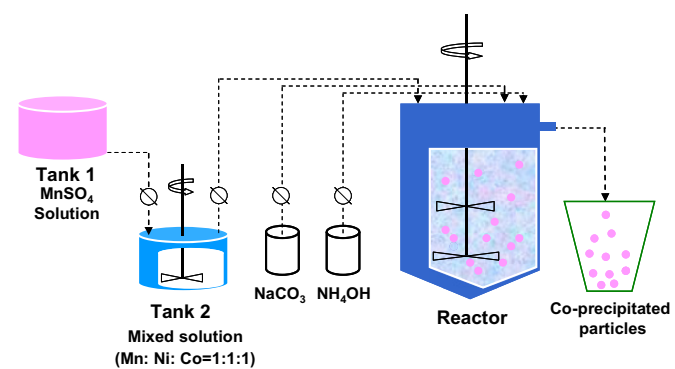
## 2. Experimental

### 2.1. Synthesis of 0.3Li<sub>2</sub>MnO<sub>3</sub>·0.7Li[Mn<sub>1/3</sub>Ni<sub>1/3</sub>Co<sub>1/3</sub>]O<sub>2</sub>

To synthesize conventional lithium-rich layered cathode material 0.3Li<sub>2</sub>MnO<sub>3</sub>·0.7Li[Mn<sub>1/3</sub>Ni<sub>1/3</sub>Co<sub>1/3</sub>]O<sub>2</sub>, MnSO<sub>4</sub>·H<sub>2</sub>O, NiSO<sub>4</sub>·6H<sub>2</sub>O and CoSO<sub>4</sub>·7H<sub>2</sub>O are used as starting materials for the co-precipitation. An aqueous mixed solution of NiSO<sub>4</sub>, CoSO<sub>4</sub>, and MnSO<sub>4</sub> (0.534:0.233:0.233 in molar ratio) with total metal ion concentration of 1.6 mol L<sup>-1</sup> was pumped into a continuously stirred tank reactor. At the same time, a 1.6 mol L<sup>-1</sup> Na<sub>2</sub>CO<sub>3</sub> solution (aq) as precipitant and the desired amount of NH<sub>4</sub>OH solution (aq) as chelating agent were also separately fed into the reactor. The concentration and pH (7.5) of the solution, the operation temperature (55 °C) and the stirring speed (800 rpm) in the reactor were carefully controlled. The obtained [Mn<sub>0.534</sub>Ni<sub>0.233</sub>Co<sub>0.233</sub>]CO<sub>3</sub> particles were then filtered, washed, and dried at 110 °C. The thus prepared carbonates were thoroughly mixed with appropriate amount of lithium carbonate and preheated at 500 °C for 8 h, and finally calcined at 900 °C for 10 h in air.

### 2.2. Synthesis of concentration-gradient material

To prepare a concentration-gradient cathode material, it is necessary to synthesize concentration-gradient precursor by co-precipitation at first. Scheme 1 shows an illustration of the co-precipitation process. A solution of MnSO<sub>4</sub> was placed in tank 1, and a mixed solution of MnSO<sub>4</sub>, NiSO<sub>4</sub> and CoSO<sub>4</sub> (Mn:Ni:Co = 1:1:1 in molar ratio) was placed in tank 2. At the beginning of the process, the aqueous solution of mixed solution from tank 2 was pumped into a continuously stirred tank reactor, where the [Mn<sub>1/3</sub>Ni<sub>1/3</sub>Co<sub>1/3</sub>]CO<sub>3</sub> core was firstly co-precipitated. When the [Mn<sub>1/3</sub>Ni<sub>1/3</sub>Co<sub>1/3</sub>]CO<sub>3</sub> particles grew to the required size, the MnSO<sub>4</sub> solution from tank 1 was slowly pumped into the mixture solution in tank 2, in which the homogeneously mixed solution was simultaneously fed into the reactor. In this way, the concentration of Mn fed into the reactor increased gradually during the reaction process. Therefore, the [Mn<sub>1/3</sub>Ni<sub>1/3</sub>Co<sub>1/3</sub>]CO<sub>3</sub> core was encapsulated completely with a stable concentration-gradient outer layer with increased manganese content. The obtained concentration-gradient precursor particles were then filtered, washed, and dried at 110 °C. Finally, a mixture of Li<sub>2</sub>CO<sub>3</sub> and the as-produced concentration-gradient precursors was



**Scheme 1.** Illustration of co-precipitation process; Tank 1: MnSO<sub>4</sub> solution. Tank 2: Mixed solution of MnSO<sub>4</sub>, NiSO<sub>4</sub> and CoSO<sub>4</sub> (Mn:Ni:Co = 1:1:1 in molar ratio).

preheated at 500 °C for 8 h, and then calcined at 900 °C for 10 h in air, to form the concentration-gradient cathode material.

### 2.3. Materials characterization

The phase identification of the samples was performed with a diffractometer (D/Max-3C, Rigaku, Japan) using Cu K $\alpha$  radiation ( $\lambda = 1.54178 \text{ \AA}$ ) and a graphite monochromator at 36 kV, 20 mA. The scanning rate was 4° min $^{-1}$  and the scanning range of diffraction angle ( $2\theta$ ) was 10° ≤ 2θ ≤ 80°. The morphology and atomic concentration of the samples were observed using a scanning electron microscopy (SEM) equipped with an energy-dispersive X-ray spectrometer (EDXS) (JSM-6100LV, JEOL, Japan). Transmission electron microscopy (TEM, FEITecnai G2, Holland) was used to investigate the crystal structure of the materials. The chemical compositions of the resulting powders were analyzed by atomic absorption spectroscopy (AAS, Vario 6 Analytik Jena AG, Jena, Germany).

### 2.4. Electrochemical test

For fabrication of the positive electrodes, the prepared materials were mixed with acetylene black, graphite and polyvinylidene fluoride (80:5:5:10) in N-methyl-2-pyrrolidone. The obtained slurry was coated onto Al foil and roll-pressed. The electrodes were dried overnight at 120 °C in a vacuum before use. Preliminary cell tests were done with a 2025 coin-type cell using Li metal as the anode. The electrolyte solution was a 1 M LiPF<sub>6</sub> in ethylene carbonate (EC)-dimethyl carbonate (DMC) (1:1, v/v). The cells were charged and discharged at different current densities using a battery cycler (Newell Battery Test) in the voltage range between 2.0 V and 4.6 V.

### 2.5. Thermal properties

For the differential scanning calorimetry (DSC) experiments, the cells were charged to 4.6 V at a current density of 20 mA g $^{-1}$  and disassembled in an Ar-filled dry box. After the remaining electrolyte was carefully removed from the surface of the electrode, the cathode materials were recovered from the current collector. Measurements were carried out in a DSC 200 PC using a temperature scan rate of 5 °C min $^{-1}$ .

## 3. Results and discussion

The lithium-rich layered cathode materials  $x\text{Li}_2\text{MnO}_3 \cdot (1-x)\text{Li}[\text{Mn}_{1/3}\text{Ni}_{1/3}\text{Co}_{1/3}]\text{O}_2$  are becoming appealing recently due to their high capacity, low cost, and improved safety compared to LiCoO<sub>2</sub> cathode [20,35]. This material is regarded as a solid solution between Li<sub>2</sub>MnO<sub>3</sub> and LiMn<sub>1/3</sub>Ni<sub>1/3</sub>Co<sub>1/3</sub>O<sub>2</sub> in different proportions. The Li<sub>2</sub>MnO<sub>3</sub> component can play an important role in stabilizing the structure of host Li[Mn<sub>1/3</sub>Ni<sub>1/3</sub>Co<sub>1/3</sub>]O<sub>2</sub> and provide additional capacity. However, the Li[Mn<sub>1/3</sub>Ni<sub>1/3</sub>Co<sub>1/3</sub>]O<sub>2</sub> is structurally unstable in high cut-off voltage when directly contacting with the electrolyte [36]. The strategy adopted in this work is based on an innovative concentration-gradient structure of the material, in which each spherical particle consists of core material Li<sub>1+x</sub>[Mn<sub>1/3</sub>Ni<sub>1/3</sub>Co<sub>1/3</sub>]O<sub>2</sub> encapsulated by a stable manganese-rich concentration-gradient outer layer. The concentration of the transition metals changed gradually from the core to the surface of the particle without any interface was expected, as illustrated in Fig. 1a. A desired concentration profile depicting the relative concentrations of Mn, Ni and Co as a function of distance from the center to the surface of the particle is shown in Fig. 1b. The concentrations of Mn, Ni and Co remain constant from the particle center to about

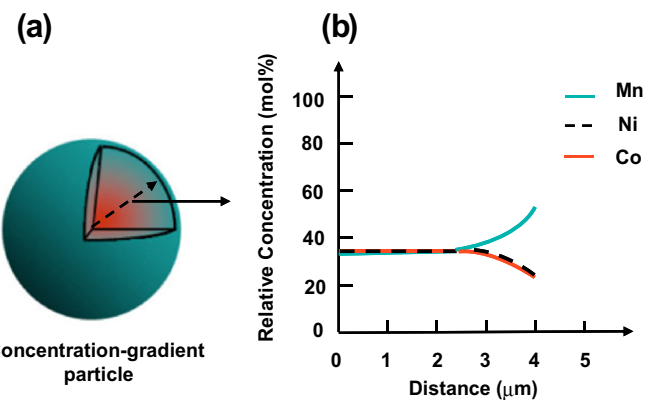
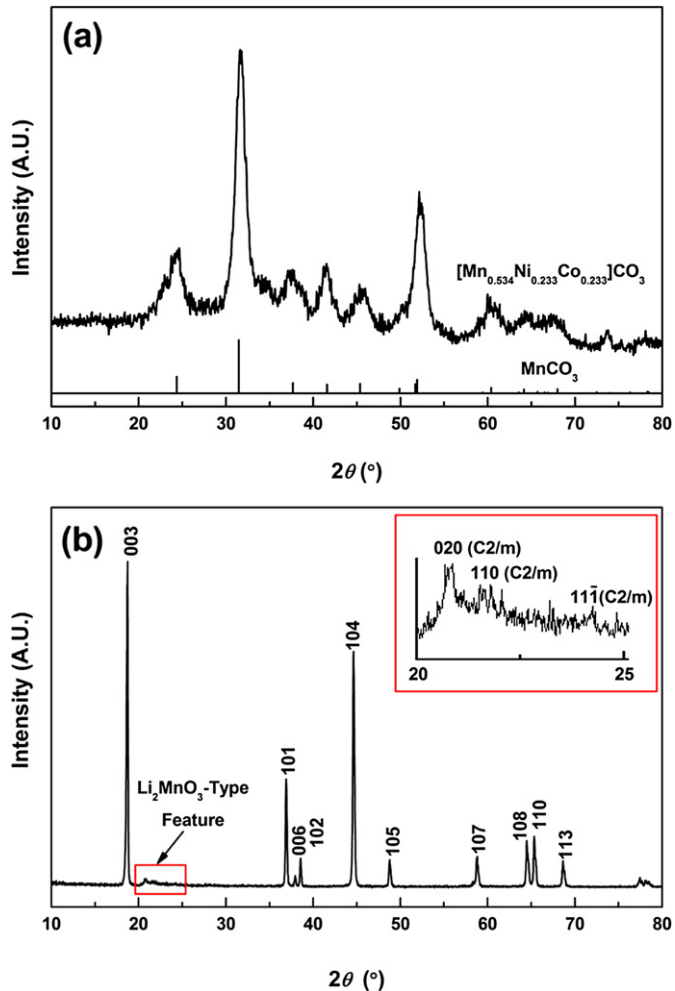


Fig. 1. (a) Schematic diagram of the concentration-gradient particle, (b) desired concentration profile depicting the relative concentrations of Mn, Ni and Co from the center to the surface of the particle.

3 μm toward the surface, and after that the Mn concentration gradually increases within the outer layer (about 1 μm). On the contrary, the concentrations of Ni and Co gradually decrease in the outer layer. In this case, the manganese-rich concentration-gradient outer layer can block the direct contact between the host Li[Mn<sub>1/3</sub>Ni<sub>1/3</sub>Co<sub>1/3</sub>]O<sub>2</sub> and the electrolyte, and the host may safely operate with no risk of structural disruption at high work voltage, as desired.

For lithium battery applications, however, a high taping-density active material is required to achieve a higher energy density because the inner space of a battery is limited. The fabrication of spherical structure particle has attracted considerable attention because of its high taping density, and co-precipitation method is one of the best approaches to synthesize spherical particles. Here, to prepare the desired spherical concentration-gradient particles, co-precipitation method was also adopted. Accordingly, the synthesis started from a spherical [Mn<sub>1/3</sub>Ni<sub>1/3</sub>Co<sub>1/3</sub>]CO<sub>3</sub> precursor, followed by its complete encapsulation by a stable concentration-gradient outer layer in which manganese content was gradually increased. The total average chemical composition of the as-prepared concentration-gradient precursor powder, determined by AAS, was found to be [Mn<sub>0.534</sub>Ni<sub>0.233</sub>Co<sub>0.233</sub>]CO<sub>3</sub>, which is well matched with the desired composition. To the final formation, the synthesized carbonate precursor was calcined with an appropriately amount of lithium carbonate at high temperature. The final lithiated oxide Li<sub>1.13</sub>[Mn<sub>0.534</sub>Ni<sub>0.233</sub>Co<sub>0.233</sub>]<sub>0.87</sub>O<sub>2</sub>, which was produced from the concentration-gradient precursor, was a solid solution between Li<sub>2</sub>MnO<sub>3</sub> and Li[Mn<sub>1/3</sub>Ni<sub>1/3</sub>Co<sub>1/3</sub>]O<sub>2</sub> with a concentration-gradient outer layer.

Fig. 2 shows the XRD patterns of the concentration-gradient [Mn<sub>0.534</sub>Ni<sub>0.233</sub>Co<sub>0.233</sub>]CO<sub>3</sub> carbonate precursor and its corresponding lithiated oxide Li<sub>1.13</sub>[Mn<sub>0.534</sub>Ni<sub>0.233</sub>Co<sub>0.233</sub>]<sub>0.87</sub>O<sub>2</sub>. As being seen in Fig. 2a, the co-precipitated carbonate is a single phase and has a typical structure corresponding to MnCO<sub>3</sub> rhodochrosite [37]. It can be indexed to a hexagonal structure with a space group of R $\bar{3}c$  [38]. The diffraction peaks, however, are broad, which may be due to the mixture of nano-scale primary particles that constitute the carbonate precursor [32,39]. After reacted with lithium carbonate at high temperature, the diffraction peaks of the resulting Li<sub>1.13</sub>[Mn<sub>0.534</sub>Ni<sub>0.233</sub>Co<sub>0.233</sub>]<sub>0.87</sub>O<sub>2</sub> become much narrower, as shown in Fig. 2b. The XRD patterns of concentration-gradient Li<sub>1.13</sub>[Mn<sub>0.534</sub>Ni<sub>0.233</sub>Co<sub>0.233</sub>]<sub>0.87</sub>O<sub>2</sub> can be indexed on the basis of the rhombohedral phase possessing the layered structure of LiNiO<sub>2</sub> (space group R $\bar{3}m$ ), except for a broad peak between 20° and 25°. These peaks are caused by superlattice ordering of the Li, Ni, Co, and Mn in the 3a site, indicating a layered structure with the monoclinic Li<sub>2</sub>MnO<sub>3</sub> character (space



**Fig. 2.** X-ray diffraction patterns for (a) concentration-gradient  $[Mn_{0.534}Ni_{0.233}Co_{0.233}]CO_3$  precursor and (b) its corresponding lithiated oxide  $Li_{1.13}[Mn_{0.534}Ni_{0.233}Co_{0.233}]_{0.87}O_2$ .

group  $C2/m$ ) [40,41]. From the inset of Fig. 2b, the monoclinic component of the concentration-gradient  $Li_{1.13}[Mn_{0.534}Ni_{0.233}Co_{0.233}]_{0.87}O_2$  material manifests itself in the appearance of three characteristic weak peaks, [020], [110] and [111], within the  $2\theta$  range 20–25°, which is consistent with other lithium-rich layered materials [16,42]. Lattice constants were calculated from the XRD pattern of Fig. 2b with a least squares refinement. The lattice constants were determined to be 0.2850(4) nm for  $\alpha$  and 1.4222(4) nm for  $c$  with a unit volume of 0.100028 nm<sup>3</sup>, using only the  $R\bar{3}m$  space group during Rietveld refinements. XRD results indicate that the final lithiated  $Li_{1.13}[Mn_{0.534}Ni_{0.233}Co_{0.233}]_{0.87}O_2$  cathode material is primarily a layered oxide with a  $Li_2MnO_3$ -type integrated phase.

The surfaces and morphologies of concentration-gradient  $[Mn_{0.534}Ni_{0.233}Co_{0.233}]CO_3$  precursor and its corresponding lithiated oxide  $Li_{1.13}[Mn_{0.534}Ni_{0.233}Co_{0.233}]_{0.87}O_2$  particle were examined using SEM. Fig. 3a and b shows the SEM images of the  $[Mn_{0.534}Ni_{0.233}Co_{0.233}]CO_3$  precursor particles. The as-prepared precursor particles appear a spherical morphology, porous structure and narrow particle size distribution. The estimated average particle diameter is about 8 μm. It is also confirmed from Fig. 3b that the micron-spherical particle of the precursor is comprised of agglomerates of nano-sized primary particles. The spherical precursor particles are similar to previous reports of carbonate particles synthesized using co-precipitation of high manganese

concentration aqueous solutions [38,43]. SEM observations of the final lithiated oxide  $Li_{1.13}[Mn_{0.534}Ni_{0.233}Co_{0.233}]_{0.87}O_2$  in Fig. 3c and d illustrates that the spherical morphology of the carbonate precursor is maintained well even after high-temperature calcinations. The estimated average particle diameter of the concentration-gradient cathode material is nearly 8 μm. Apparently, the concentration-gradient  $Li_{1.13}[Mn_{0.534}Ni_{0.233}Co_{0.233}]_{0.87}O_2$  particle represents a good crystalline, and the size of the primary particles increases obviously compared to that of the precursor, which is consistent with previous reports [32,44].

To directly observe the internal morphology and determine the local composition in the as-prepared particles, the particles were firstly embedded in a resin and cut by a focused ion beam, and then SEM and EDXS on a cross-section of the concentration-gradient  $[Mn_{0.534}Ni_{0.233}Co_{0.233}]CO_3$  precursor and its corresponding lithiated oxide  $Li_{1.13}[Mn_{0.534}Ni_{0.233}Co_{0.233}]_{0.87}O_2$  particle were conducted, as shown in Fig. 4. As seen in Fig. 4a, the precursor particle is quite homogeneous, and the core is tightly bonded by a concentration-gradient outer layer with no apparent interface. After high-temperature calcinations process, the final lithiated oxide  $Li_{1.13}[Mn_{0.534}Ni_{0.233}Co_{0.233}]_{0.87}O_2$  particle is also quite homogeneous without any obvious gap between the inner core and the concentration-gradient outer layer (Fig. 4b), suggesting that the continuous gradient in composition could potentially help to mitigate separation that could occur between two chemically distinct regions with particles [34]. Also, the taping density of the prepared concentration-gradient material is quite high, approximately 2.24 g cm<sup>-3</sup>. To track the compositional change, EDXS signals were obtained across the radius of the precursor and final lithiated oxide particle at nine positions. The concentrations of Mn, Ni, and Co were plotted as a function of distance from the core center to surface of the particle, as illustrated in Fig. 4c and d. From the Fig. 4c, the precursor core is composed of a molar ratio of 0.34 Mn, 0.33 Ni, and 0.33 Co, and the concentrations of Mn, Ni, and Co remain almost constant throughout the core, which is consistent with the initially designed. After that, the molar concentration of Mn gradually increases to 0.54 near the outer layer surface. By contrast, the Ni and Co concentrations decrease to 0.24 and 0.22, respectively, resulting in a surface composition of  $[Mn_{0.54}Ni_{0.24}Co_{0.22}]CO_3$ . EDXS measurements performed at points on the cross-sectioned of final lithiated oxide  $Li_{1.13}[Mn_{0.534}Ni_{0.233}Co_{0.233}]_{0.87}O_2$  particle from the interior to the surface confirm that a gradient outer layer in the transition metal composition is maintained after lithiation/calcinations, as illustrated in Fig. 4d. The molar concentrations of Mn, Ni, and Co in the final lithiated oxide remain almost constant from the particle center to about 3 μm toward the surface (that is the core), though the molar concentration of Mn is slightly higher compared to the precursor material (from 0.34 to 0.37). Subsequently, the Mn concentration gradually increases to 0.48 at the particle surface, while the concentrations of Ni and Co decrease to 0.27 and 0.25, respectively. The concentration variation in the lithiated oxide is less steep than in the precursor due to inter-diffusion of transition metals during the high temperature calcinations. However, a concentration-gradient outer layer in transition metal composition is maintained in the final lithiated oxide. Based on above results, it is confirmed that the lithium-rich layered  $Li_{1.13}[Mn_{0.534}Ni_{0.233}Co_{0.233}]_{0.87}O_2$  cathode material, which is consisted of an inner core and a stable concentration-gradient outer layer, is successfully synthesized as desired.

The microstructure of the concentration-gradient  $Li_{1.13}[Mn_{0.534}Ni_{0.233}Co_{0.233}]_{0.87}O_2$  cathode material was investigated by TEM and HRTEM tests. The powder sample was firstly ground and fractured pieces from individual spherical particle before placed on a carbon film-coated TEM grid. Fig. 5a and b shows the low magnification TEM images of primary particles in the core and on the surface

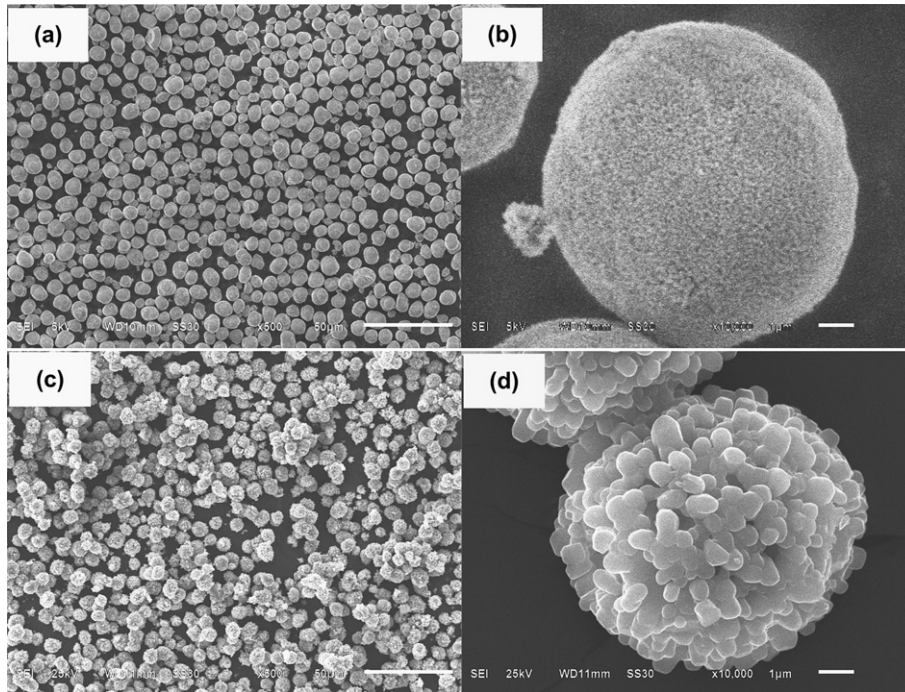


**Fig. 3.** SEM images of (a,b) concentration-gradient [Mn<sub>0.534</sub>Ni<sub>0.233</sub>Co<sub>0.233</sub>]CO<sub>3</sub> precursor and (c,d) its corresponding lithiated oxide Li<sub>1.13</sub>[Mn<sub>0.534</sub>Ni<sub>0.233</sub>Co<sub>0.233</sub>]<sub>0.87</sub>O<sub>2</sub>.

position of the concentration-gradient spherical particle, respectively. The dispersive primary particles are submicron and/or nano-scaled in diameter, which is in agreement with the SEM observation in Fig. 3d. The HRTEM micrographs of selected area in Fig. 5a and b are shown in Fig. 5c and d, respectively, and the insets are the corresponding selected area electron diffraction (SAED) patterns (subscripts R and M are related to rhombohedral and monoclinic

phases, respectively). Parallel lattice in Fig. 5c corresponds to the typical layered materials with interplanar distances of about 4.7 Å which corresponds to the distances of the close packed [003] planes of the R<sub>3</sub>m layered structure. The corresponding SAED pattern in the inset of Fig. 5c also suggests that the crystal structure in the core area of the concentration-gradient particle is relatively pure rhombohedral structure. This may be due to the significantly less

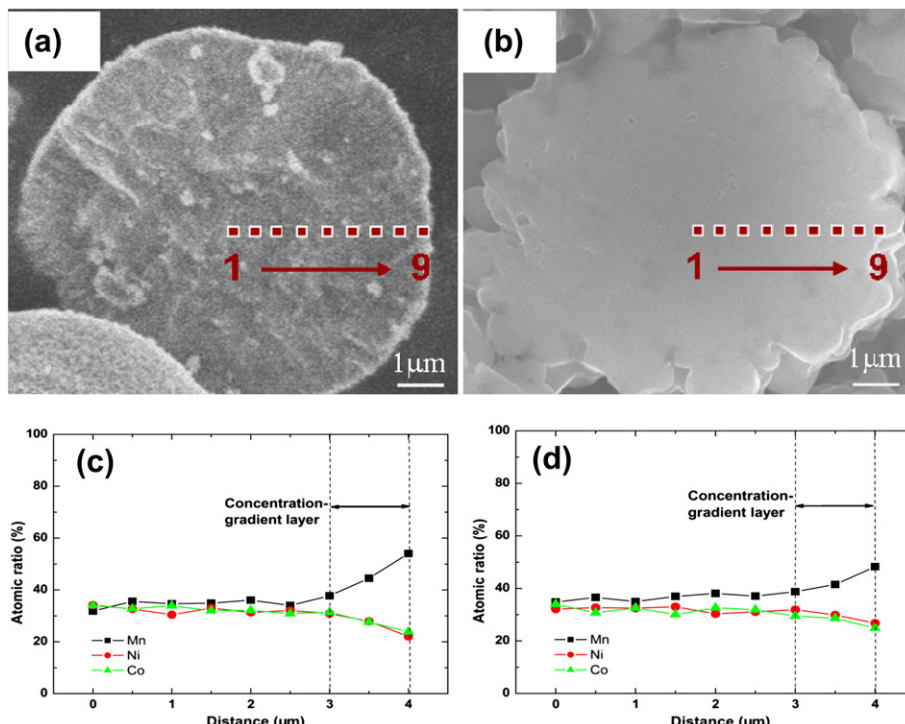


**Fig. 4.** Cross-sectional SEM images of (a) concentration-gradient [Mn<sub>0.534</sub>Ni<sub>0.233</sub>Co<sub>0.233</sub>]CO<sub>3</sub> precursor and (b) its corresponding lithiated oxide Li<sub>1.13</sub>[Mn<sub>0.534</sub>Ni<sub>0.233</sub>Co<sub>0.233</sub>]<sub>0.87</sub>O<sub>2</sub>. EDXS compositional change from the cross-section of (c) precursor particle and (d) final lithiated oxide particle on the labeled points 1 through 9.

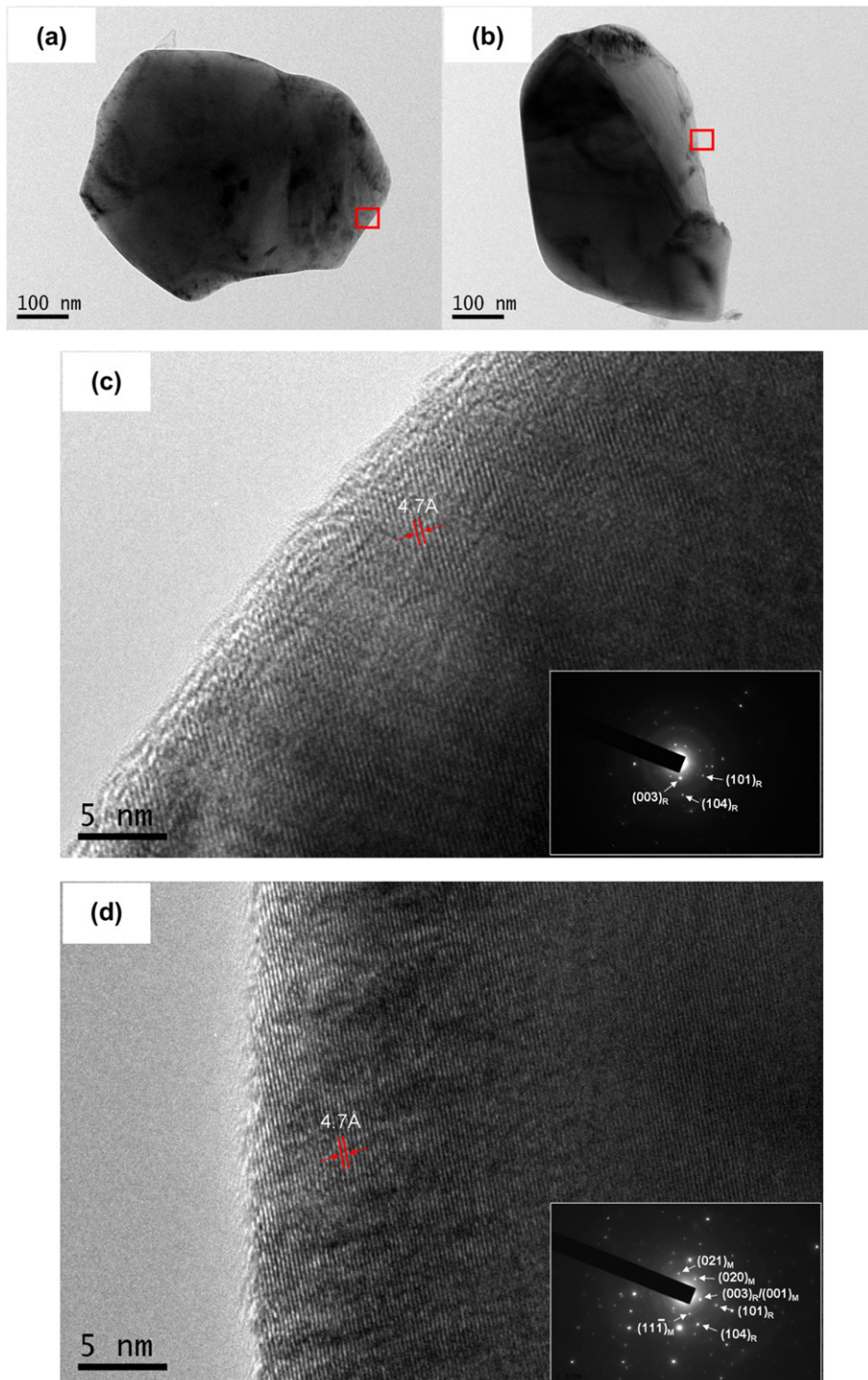


**Fig. 5.** (a), (c) TEM and HRTEM images of primary particle in the inner core, and (b), (d) on the surface of the spherical concentration-gradient  $\text{Li}_{1.13}[\text{Mn}_{0.534}\text{Ni}_{0.233}\text{Co}_{0.233}]_{0.87}\text{O}_2$  particle; the insert of (c) and (d) are the corresponding SAED pattern; the indexes marked by subscripts R and M are related to rhombohedral and monoclinic phases, respectively.

manganese content in the core area of the concentration-gradient particle, so it is more difficult to cluster the lithium distinctly around the manganese ions to generate short-range order in the  $\text{LiMn}_{6-x}\text{M}_x$  hexagonal units ( $\text{M} = \text{Ni, Co}$ ), resulting in restrict the growth and size of the  $\text{Li}_2\text{MnO}_3$ -like regions in the transition metal-rich layers [39,42]. However, both structures, rhombohedral and monoclinic, are present in the surface primary particle of the concentration-gradient material, while it is difficult to distinguish from one another in the HRTEM image (Fig. 5d). Only  $[003]_R$  and

$[001]_M$  lattice fringes with the characteristic spacing of 4.7 Å are clearly detectable in Fig. 5d. As evident in insert of Fig. 5d, however, it can clear distinguish between rhombohedral and monoclinic components from the SEAD pattern. It seems reasonable to suggest that these areas are associated with nanovolumes of the rhombohedral  $\text{LiNiO}_2$ -like and monoclinic  $\text{Li}_2\text{MnO}_3$  structures that are in intimate contact, as is concluded with the approach presented by other researchers [2,45]. By above knowable, the monoclinic  $\text{Li}_2\text{MnO}_3$  structures in the concentration-gradient particles are

unequally distributed. There are no/less monoclinic  $\text{Li}_2\text{MnO}_3$  structures in the core area of the concentration-gradient particles due to the less manganese content. With the increase of the Mn concentration in the outer layer of the concentration-gradient particles, the microstructure in this area is composed of nanodomains of both rhombohedral  $\text{LiNiO}_2$ -like and monoclinic  $\text{Li}_2\text{MnO}_3$  structures, which are integrated and interconnected with one another at the atomic level.

The electrochemical properties of the concentration-gradient  $\text{Li}_{1.13}[\text{Mn}_{0.534}\text{Ni}_{0.233}\text{Co}_{0.233}]_{0.87}\text{O}_2$  were compared with those of the conventional material  $0.3\text{Li}_2\text{MnO}_3 \cdot 0.7\text{Li}[\text{Mn}_{1/3}\text{Ni}_{1/3}\text{Co}_{1/3}]\text{O}_2$  based on tests using the 2025 coin-type half cell employing Li metal as the anode. Fig. 6 displays the voltage profile of the first and second charge–discharge of  $\text{Li}/0.3\text{Li}_2\text{MnO}_3 \cdot 0.7\text{Li}[\text{Mn}_{1/3}\text{Ni}_{1/3}\text{Co}_{1/3}]\text{O}_2$  and Li/concentration-gradient  $\text{Li}_{1.13}[\text{Mn}_{0.534}\text{Ni}_{0.233}\text{Co}_{0.233}]_{0.87}\text{O}_2$  cells cycled between 2.0 V and 4.6 V at a rate of 0.1 C (1 C corresponds to 200 mA g<sup>−1</sup> current density) at room temperature. The concentration-gradient electrode delivers an initial discharge capacity of 220 mAh g<sup>−1</sup>, which do not seem to significantly alter its specific capacity compared to the  $0.3\text{Li}_2\text{MnO}_3 \cdot 0.7\text{Li}[\text{Mn}_{1/3}\text{Ni}_{1/3}\text{Co}_{1/3}]\text{O}_2$  electrode (223 mAh g<sup>−1</sup>). In addition, both the as-prepared samples exhibit two distinguished voltage plateau during the initial charge process. The first voltage plateau at voltage <4.5 V, which is corresponds to lithium extraction from  $\text{Li}[\text{Mn}_{1/3}\text{Ni}_{1/3}\text{Co}_{1/3}]\text{O}_2$  component with the concomitant oxidation of  $\text{Ni}^{2+}/\text{Ni}^{4+}$  and  $\text{Co}^{3+}/\text{Co}^{4+}$ , and the second plateau is consistent with the removal of lithium from  $\text{Li}_2\text{MnO}_3$  component of the electrode structure accompanied by oxygen evolution when charged above 4.5 V [46,47]. Interestingly, the ~4.5 V potential voltage disappears in the second charging process. The reason is that the removal of “ $\text{Li}_2\text{O}$ ” from  $\text{Li}_2\text{MnO}_3$  component is irreversible, which is also the main reason for irreversible capacity loss on the initial cycle for lithium-rich layered cathode materials [48,49]. Similar charge–discharge behavior for the first two cycled described above has been reported for other lithium-rich layered materials [16,42].

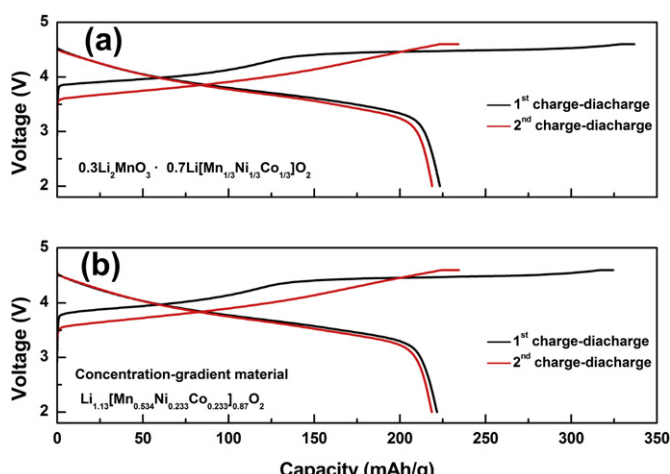
The  $dQ/dV$  plots of the charge–discharge curves in Fig. 6a and b are shown in Fig. 7a and b, respectively, several features are particularly noteworthy. During the initial charge to 4.6 V, both of the electrodes exhibit two distinct  $dQ/dV$  peaks, one is from 3.7 V to 4.25 V and the other is from 4.25 V to 4.6 V. The anodic peaks positioned at about 3.9 V during the first charge is due to

the oxidation of  $\text{Ni}^{2+}$  to  $\text{Ni}^{4+}$  and  $\text{Co}^{3+}$  to  $\text{Co}^{4+}$ , which are correspond to the voltage slope at voltage <4.5 V in Fig. 6. The much larger anodic peak at ~4.5 V is the irreversible reaction in which the lithium is extracted from  $\text{Li}_2\text{MnO}_3$  component with the simultaneous release of oxygen corresponding to the long ~4.5 V plateau in Fig. 6 [50]. During the second cycle, the larger anodic peak at ~4.5 V disappears, and the anodic peak at ~3.9 V shifts to ~3.8 V position, indicating that the bulk material structure and/or the electrode/electrolyte interface have been modified after the first cycle. In addition, the  $\text{Li}/0.3\text{Li}_2\text{MnO}_3 \cdot 0.7\text{Li}[\text{Mn}_{1/3}\text{Ni}_{1/3}\text{Co}_{1/3}]\text{O}_2$  cell shows weak cathodic peak at around 3.25 V in the second cycle (see Fig. 7a). It is possible that this peak could correspond to the reduction of a small amount of  $\text{Mn}^{4+}$  ion [51]. However, there is no cathodic peak at ~3.25 V in the Li/concentration-gradient  $\text{Li}_{1.13}[\text{Mn}_{0.534}\text{Ni}_{0.233}\text{Co}_{0.233}]_{0.87}\text{O}_2$  cell (see Fig. 7b). This behavior implies that for Li/concentration-gradient  $\text{Li}_{1.13}[\text{Mn}_{0.534}\text{Ni}_{0.233}\text{Co}_{0.233}]_{0.87}\text{O}_2$  electrode, noticeable structural degradation does not take place during the cycling process.

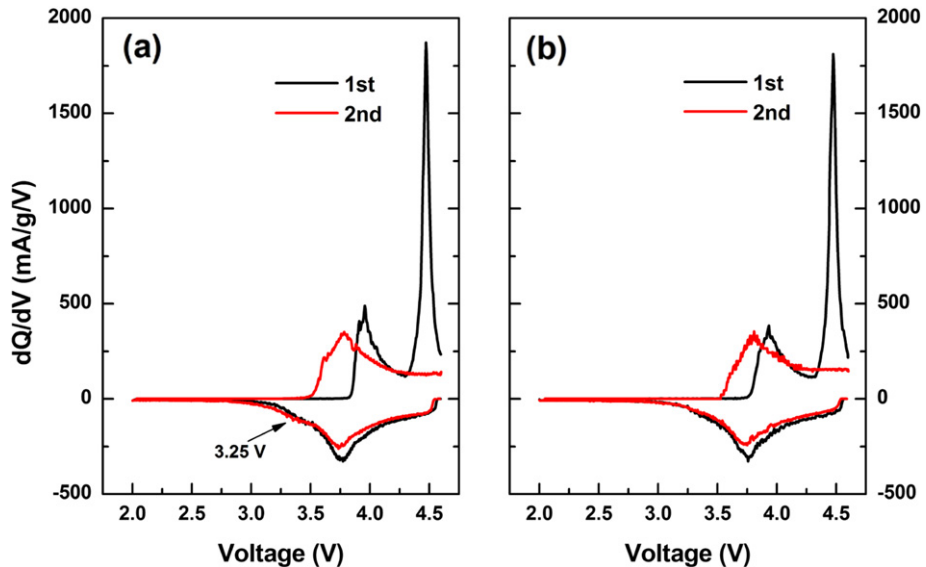
Fig. 8 shows the continuous charge–discharge curves and cyclabilities of the lithium-rich layered  $0.3\text{Li}_2\text{MnO}_3 \cdot 0.7\text{Li}[\text{Mn}_{1/3}\text{Ni}_{1/3}\text{Co}_{1/3}]\text{O}_2$  and concentration-gradient  $\text{Li}_{1.13}[\text{Mn}_{0.534}\text{Ni}_{0.233}\text{Co}_{0.233}]_{0.87}\text{O}_2$  electrodes at 25 °C. The cells were first charged/discharged at a rate of 0.1 C, and then cycled at a rate of 0.5 C in the voltage range of 2.0–4.6 V. As being seen in Fig. 8, the  $0.3\text{Li}_2\text{MnO}_3 \cdot 0.7\text{Li}[\text{Mn}_{1/3}\text{Ni}_{1/3}\text{Co}_{1/3}]\text{O}_2$  cell exhibits gradually capacity fading upon cycling at 25 °C, and the capacity retention is only 83.4% over 100 cycles. On the other hand, the concentration-gradient  $\text{Li}_{1.13}[\text{Mn}_{0.534}\text{Ni}_{0.233}\text{Co}_{0.233}]_{0.87}\text{O}_2$  cell shows excellent capacity retention, maintaining 97.2% of its initial capacity after 100 cycles. In order to further evaluate the stability of the as-prepared new concentration-gradient material, the cells were cycled at elevated temperature 55 °C, as shown in Fig. 9. The cells based on both  $0.3\text{Li}_2\text{MnO}_3 \cdot 0.7\text{Li}[\text{Mn}_{1/3}\text{Ni}_{1/3}\text{Co}_{1/3}]\text{O}_2$  material and concentration-gradient  $\text{Li}_{1.13}[\text{Mn}_{0.534}\text{Ni}_{0.233}\text{Co}_{0.233}]_{0.87}\text{O}_2$  material show higher initial capacity at 55 °C than those of at 25 °C. However, the  $\text{Li}/0.3\text{Li}_2\text{MnO}_3 \cdot 0.7\text{Li}[\text{Mn}_{1/3}\text{Ni}_{1/3}\text{Co}_{1/3}]\text{O}_2$  cell retains only 72.3% of its initial capacity after 50 cycles, whereas the Li/concentration-gradient  $\text{Li}_{1.13}[\text{Mn}_{0.534}\text{Ni}_{0.233}\text{Co}_{0.233}]_{0.87}\text{O}_2$  cell shows superior capacity retention of 92.4% during the same cycling period. These results clearly indicate that the outer layer with manganese concentration-gradient is responsible for the significant improvement of the cycle characteristics. That is, the stable outer layer can block the direct contact between the host  $\text{Li}[\text{Mn}_{1/3}\text{Ni}_{1/3}\text{Co}_{1/3}]\text{O}_2$  material and electrolyte, especially reducing dissolution of  $\text{Co}^{4+}$ , and thus reducing capacity loss, even at elevated temperature.

Fig. 10 presents the rate capability of  $\text{Li}/0.3\text{Li}_2\text{MnO}_3 \cdot 0.7\text{Li}[\text{Mn}_{1/3}\text{Ni}_{1/3}\text{Co}_{1/3}]\text{O}_2$  and Li/concentration-gradient  $\text{Li}_{1.13}[\text{Mn}_{0.534}\text{Ni}_{0.233}\text{Co}_{0.233}]_{0.87}\text{O}_2$  cells between 2.0 and 4.6 V at room temperature. Each cell was charged at a rate of 0.1 C and then discharged at different rates from 0.1 C to 2 C. As being seen in Fig. 10, the concentration-gradient  $\text{Li}_{1.13}[\text{Mn}_{0.534}\text{Ni}_{0.233}\text{Co}_{0.233}]_{0.87}\text{O}_2$  cell shows better rate capability than  $0.3\text{Li}_2\text{MnO}_3 \cdot 0.7\text{Li}[\text{Mn}_{1/3}\text{Ni}_{1/3}\text{Co}_{1/3}]\text{O}_2$  cell. As the current density increased from 0.1 C to 2 C, the discharge capacity of the concentration-gradient cell drops from 220 mAh g<sup>−1</sup> to 161 mAh g<sup>−1</sup>, while that of the conventional cell delivers 223 mAh g<sup>−1</sup> at 0.1 C and 144 mAh g<sup>−1</sup> at 2 C. The enhanced rate capacity of the concentration-gradient  $\text{Li}_{1.13}[\text{Mn}_{0.534}\text{Ni}_{0.233}\text{Co}_{0.233}]_{0.87}\text{O}_2$  may be caused by the excess  $\text{Li}^+$  ions incorporated in the layered structure of the core area, resulting in reduce cation mixing between  $\text{Ni}^{2+}$  and  $\text{Li}^+$  ions [52,53].

When a positive electrode material is considered in commercial applications, particularly in HEVs and PHEVs, the thermal stability of the materials is of critical importance. Fig. 11 shows differential scanning calorimetry (DSC) curves of the concentration-gradient



**Fig. 6.** Initial and second charge–discharge profiles for (a)  $\text{Li}/0.3\text{Li}_2\text{MnO}_3 \cdot 0.7\text{Li}[\text{Mn}_{1/3}\text{Ni}_{1/3}\text{Co}_{1/3}]\text{O}_2$ , and (b) Li/concentration-gradient  $\text{Li}_{1.13}[\text{Mn}_{0.534}\text{Ni}_{0.233}\text{Co}_{0.233}]_{0.87}\text{O}_2$  coin cells between 2.0 V and 4.6 V at a rate of 0.1 C.



**Fig. 7.** Differential capacity versus voltage of (a)  $Li/0.3Li_2MnO_3 \cdot 0.7Li[Mn_{1/3}Ni_{1/3}Co_{1/3}]O_2$  and (b)  $Li/concentration\text{-gradient } Li_{1.13}[Mn_{0.534}Ni_{0.233}Co_{0.233}]_{0.87}O_2$  coin cells cycled between 2.0 V and 4.6 V at a rate of 0.1 C.

$Li_{1.13}[Mn_{0.534}Ni_{0.233}Co_{0.233}]_{0.87}O_2$  in comparison with  $0.3Li_2MnO_3 \cdot 0.7Li[Mn_{1/3}Ni_{1/3}Co_{1/3}]O_2$  cathode material. Both materials were charged to 4.6 V under the same rate of 0.1 C. The  $0.3Li_2MnO_3 \cdot 0.7Li[Mn_{1/3}Ni_{1/3}Co_{1/3}]O_2$  electrode exhibits a large exothermic peak at

242 °C with a heat generation of 914 J g<sup>-1</sup>. Meanwhile, the concentration-gradient  $Li_{1.13}[Mn_{0.534}Ni_{0.233}Co_{0.233}]_{0.87}O_2$  electrode shows an improved thermal stability with an exothermic reaction at 264 °C and much reduced heat generation of 536 J g<sup>-1</sup>. This result

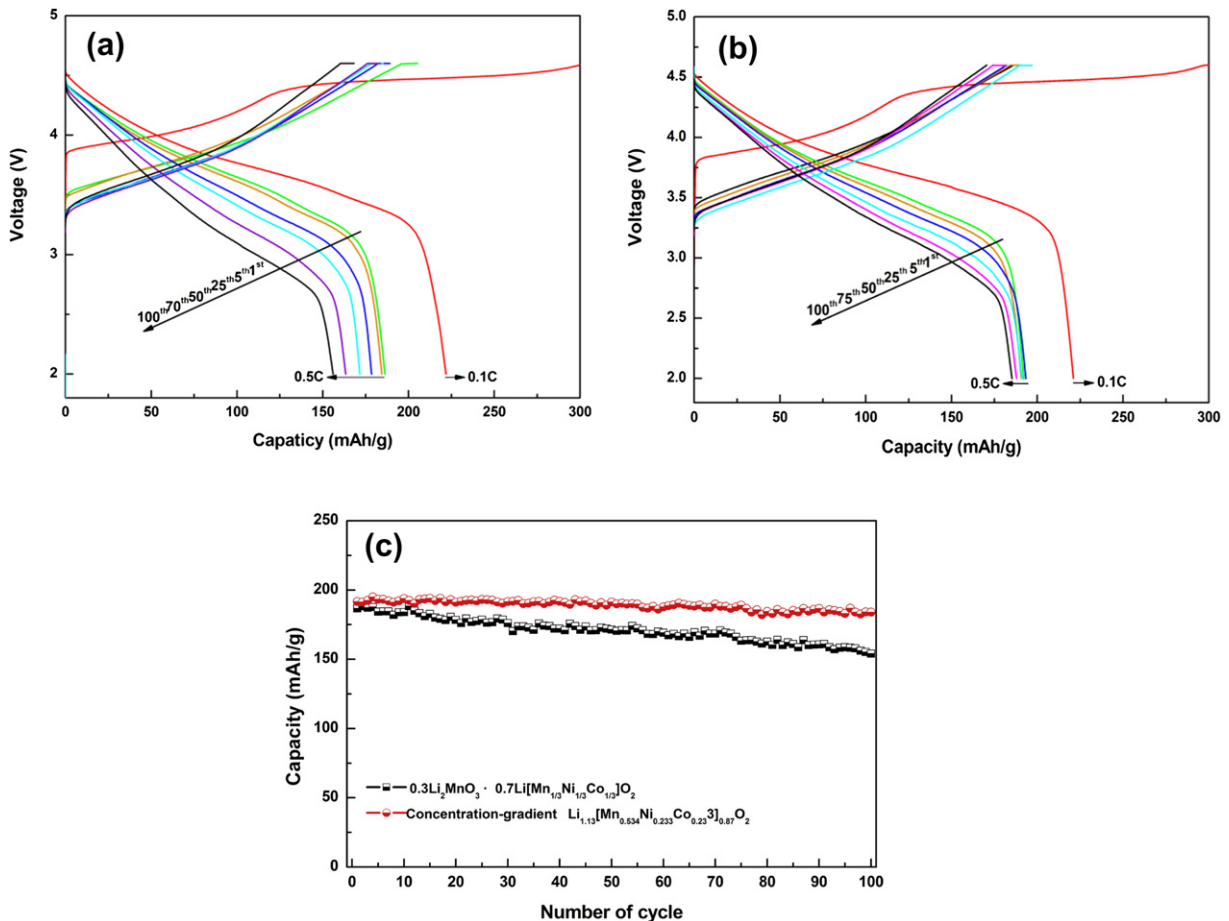


**Fig. 8.** Continuous charge and discharge curves of (a)  $0.3Li_2MnO_3 \cdot 0.7Li[Mn_{1/3}Ni_{1/3}Co_{1/3}]O_2$ , (b) concentration-gradient  $Li_{1.13}[Mn_{0.534}Ni_{0.233}Co_{0.233}]_{0.87}O_2$  cells and (c) discharge capacity versus cycle number of Li/(a), (b) cells at 25 °C between 2.0 V and 4.6 V at a rate of 0.5 C.

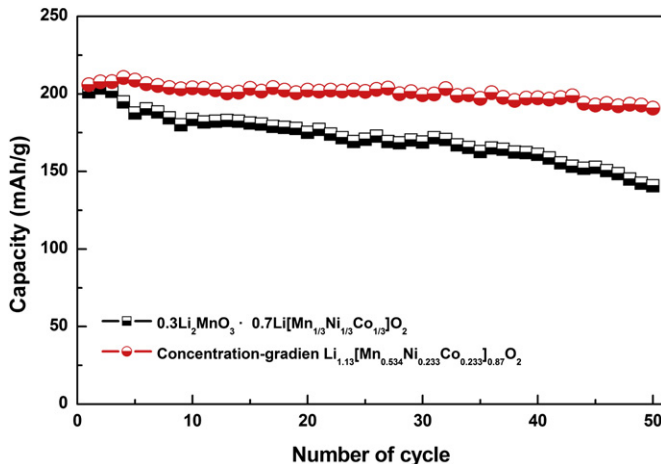


**Fig. 9.** Discharge capacity versus cycle number of  $\text{Li}/0.3\text{Li}_2\text{MnO}_3 \cdot 0.7\text{Li}[\text{Mn}_{1/3}\text{Ni}_{1/3}\text{Co}_{1/3}]_{\text{O}_2}$  and  $\text{Li}/\text{concentration-gradient } \text{Li}_{1.13}[\text{Mn}_{0.534}\text{Ni}_{0.233}\text{Co}_{0.233}]_{0.87}\text{O}_2$  cells at  $55^{\circ}\text{C}$  between  $2.0\text{ V}$  and  $4.6\text{ V}$  at a rate of  $0.5\text{ C}$ .

clearly indicates that the outer layer with manganese concentration-gradient is responsible for the significant improvement of the thermal characteristics. That is, the thermally stable outer layer could tightly encapsulate the core material, so that the unstable host  $\text{Li}_{1-\delta}[\text{Mn}_{1/3}\text{Ni}_{1/3}\text{Co}_{1/3}]_{\text{O}_2}$  does not directly contact the electrolyte.

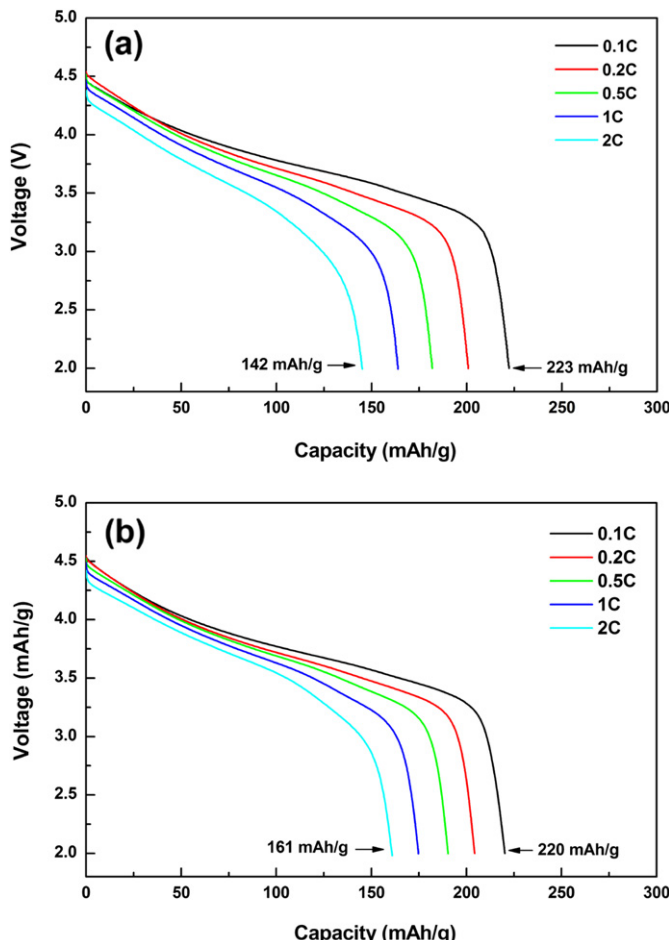


**Fig. 10.** Discharge curves from  $4.6\text{ V}$  to  $2.0\text{ V}$  at various rates of (a)  $\text{Li}/0.3\text{Li}_2\text{MnO}_3 \cdot 0.7\text{Li}[\text{Mn}_{1/3}\text{Ni}_{1/3}\text{Co}_{1/3}]_{\text{O}_2}$  and (b)  $\text{Li}/\text{concentration-gradient } \text{Li}_{1.13}[\text{Mn}_{0.534}\text{Ni}_{0.233}\text{Co}_{0.233}]_{0.87}\text{O}_2$  coin cells.

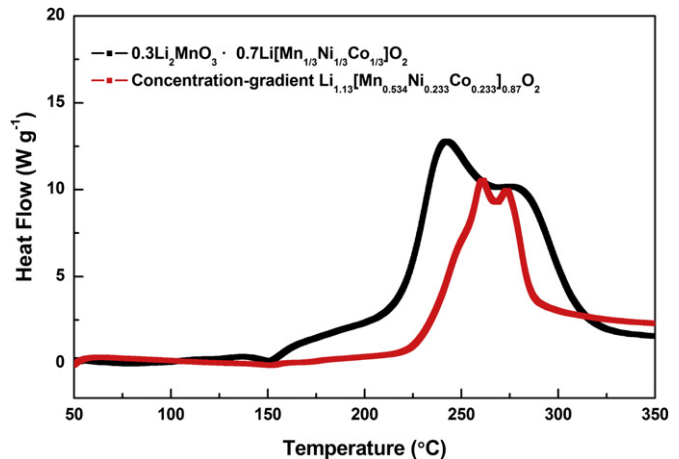


**Fig. 11.** DSC curves of  $0.3\text{Li}_2\text{MnO}_3 \cdot 0.7\text{Li}[\text{Mn}_{1/3}\text{Ni}_{1/3}\text{Co}_{1/3}]_{\text{O}_2}$  and concentration-gradient  $\text{Li}_{1.13}[\text{Mn}_{0.534}\text{Ni}_{0.233}\text{Co}_{0.233}]_{0.87}\text{O}_2$  cathode material.

#### 4. Conclusions

The lithium-rich layered cathode material  $\text{Li}_{1.13}[\text{Mn}_{0.534}\text{Ni}_{0.233}\text{Co}_{0.233}]_{0.87}\text{O}_2$ , which was consisted of an inner core and a stable manganese-rich concentration-gradient outer layer, has been prepared by co-precipitation method. The concentration-gradient  $\text{Li}_{1.13}[\text{Mn}_{0.534}\text{Ni}_{0.233}\text{Co}_{0.233}]_{0.87}\text{O}_2$  exhibits a very high discharge capacity of  $220\text{ mAh g}^{-1}$  between  $2.0\text{ V}$  and  $4.6\text{ V}$  at a rate of  $0.1\text{ C}$ , and shows excellent lithium intercalation stability with capacity retention of  $97.2\%$  after  $100$  cycles at a rate of  $0.5\text{ C}$  at  $25^{\circ}\text{C}$ . At elevated temperature  $55^{\circ}\text{C}$ , the concentration-gradient  $\text{Li}_{1.13}[\text{Mn}_{0.534}\text{Ni}_{0.233}\text{Co}_{0.233}]_{0.87}\text{O}_2$  also exhibits excellent cyclability with a capacity retention of  $92.4\%$  over  $50$  cycles, while the conventional material with the same composition retains only  $72.3\%$  of its initial capacity during the same cycling period at a rate of  $0.5\text{ C}$ . Besides, the concentration-gradient material shows much improved thermal stability with an exothermic reaction at  $264^{\circ}\text{C}$  and much low heat generation of  $536\text{ J g}^{-1}$ . The enhanced performance of the concentration-gradient material is due to the stabilization of manganese-rich concentration-gradient outer layer. The lithium-rich layered material with a stable manganese-rich concentration-gradient outer layer as a new positive electrode material is a significant breakthrough in the development of advanced lithium ion batteries with a high energy, long cycle life, and safety.

#### Acknowledgments

This work was funded by the National Natural Science Foundation of China under project No. 20871101, Scientific Research Fund of Hunan Provincial Education Department No. 09C947, Key Project of Science and Technology Department of Hunan Province Government under project No. 2009WK2007, Colleges and Universities in Hunan Province plans to graduate research and innovation under project No. CX2009B133.

#### References

- [1] A. Manthiram, *J. Phys. Chem. Lett.* 2 (2011) 176–184.
- [2] M.M. Thackeray, S.H. Kang, C.S. Johnson, J.T. Vaughan, R. Benedek, S.A. Hackney, *J. Mater. Chem.* 17 (2007) 3112–3125.
- [3] G.B. Zhong, Y.Y. Wang, Y.Q. Yu, C.H. Chen, *J. Power Sources* 205 (2012) 385–393.
- [4] C. Delmas, G. Prado, A. Rougier, E. Suard, L. Fournes, *Solid State Ionics* 135 (2000) 71–79.
- [5] C. Jaephil, P. Byungwoo, *J. Power Sources* 92 (2001) 35–39.
- [6] T. Ohzuku, N. Yabuuchi, *J. Power Sources* 171 (2003) 119–121.

- [7] K.S. Lee, S.T. Myung, Y.-K. Sun, *J. Power Sources* 195 (2010) 6043–6048.
- [8] Y.P. Wu, Elke Rahmb, Rudolf Holze, *Electrochim. Acta* 47 (2002) 3491–3507.
- [9] V. Subramanian, G.T.K. Fey, *Solid State Ionics* 148 (2002) 351–358.
- [10] S. Madhavi, G.V. Subba Rao, B.V.R. Chowdari, S.F.Y. Li, *Solid State Ionics* 152 (2002) 199–205.
- [11] H. Liu, J. Li, Z.G. Zhang, Z.L. Gong, Y. Yang, *Electrochim. Acta* 49 (2004) 1151–1159.
- [12] K.K. Lee, W.S. Yoon, K.B. Kim, K.Y. Lee, S.T. Hong, *J. Power Sources* 97 (2001) 308–312.
- [13] H.S. Shin, S.H. Park, C.S. Yoon, Y.K. Sun, *Electrochim. Solid-state Lett.* 8 (2005) A559–A563.
- [14] J.S. Kim, C.S. Johnson, M.M. Thackeray, *Electrochim. Commun.* 4 (2002) 205–209.
- [15] J.S. Kim, C.S. Johnson, J.T. Vaughey, M.M. Thackeray, S.A. Hackney, W. Yoon, C.P. Grey, *Chem. Mater.* 16 (2004) 1996–2006.
- [16] M.M. Thackeray, C.S. Johnson, J.T. Vaughey, N. Li, S.A. Hackney, *J. Mater. Chem.* 15 (2005) 2257–2267.
- [17] C.R. Fell, D.H. Lee, Y.S. Meng, J.M. Gallardo-Amores, E. Moran, M.E. Arroyo-de Dompablo, *Energy Environ. Sci.* 5 (2012) 6214–6224.
- [18] Z. Lu, D.D. MacNeil, J.R. Dahn, *Electrochim. Solid-state Lett.* 4 (2001) A191–A194.
- [19] J. Breger, Y.S. Meng, Y. Hinuma, S. Kumar, K. Kang, *Chem. Mater.* 18 (2006) 4768–4781.
- [20] C.S. Johnson, N. Li, C. Lefief, M.M. Thackeray, *Electrochim. Commun.* 9 (2007) 787–795.
- [21] G.G. Amatucci, M.M. Tarascon, C. Klein, *Solid State Ionics* 83 (1996) 167–173.
- [22] J. Shim, R. Kostecki, T. Richardson, X. Song, K.A. Striebel, *J. Power Sources* 112 (2002) 222–230.
- [23] J. Zheng, J. Li, Z. Zhang, X. Guo, Y. Yang, *Solid State Ionics* 179 (2008) 1794–1799.
- [24] G.Y. Kim, *J. Appl. Electrochem.* 38 (2008) 1477–1481.
- [25] J. Gao, J. Kim, A. Manthiram, *Electrochim. Commun.* 11 (2009) 84–86.
- [26] Nupur Nikkan. Sinha, N. Munichandraiah, *ACS Appl. Mater. Interfaces* 1 (2009) 1241–1249.
- [27] C. Venkateswara Rao, A. Leela Mohana Reddy, Y. Ishikawa, P.M. Ajayan, *ACS Appl. Mater. Interfaces* 3 (2011) 2966–2972.
- [28] C. Li, H.P. Zhang, L.J. Fu, H. Liu, Y.P. Wu, E. Rahmb, R. Holze, H.Q. Wu, *Electrochim. Acta* 51 (2006) 3872–3883.
- [29] S.-T. Myung, K.-S. Lee, D.-W. Kim, B. Scrosati, Y.-K. Sun, *Energy Environ.* 4 (2011) 935–939.
- [30] Y.-K. Sun, D.-H. Kim, C.S. Yoon, S.-T. Myung, J. Prakash, K. Amine, *Adv. Funct. Mater.* 20 (2010) 485–491.
- [31] K. Kang, Y.S. Meng, J. Breger, C.P. Grey, G. Ceder, *Science* 311 (2006) 977–980.
- [32] H. Deng, I. Belharouak, H. Wu, D. Dambournet, K. Amine, *J. Electrochem. Soc.* 157 (2010) A776–A781.
- [33] Y.-K. Sun, S.-T. Myung, M.-H. Kim, J. Prakash, K. Amine, *J. Am. Chem. Soc.* 127 (2005) 13411–13418.
- [34] Y.-K. Sun, S.-T. Myung, B.-C. Park, K. Amine, *Chem. Mater.* 18 (2006) 5159–5163.
- [35] Y. Wu, A. Manthiram, *Electrochim. Solid-state Lett.* 9 (2006) A221–A224.
- [36] L.Y. Yu, W.H. Qiu, F. Lian, W. Liu, X.L. Kang, J.Y. Huang, *Mater. Lett.* 62 (2008) 3010–3013.
- [37] S.-M. Park, T.-H. Cho, M. Yoshido, *Chem. Lett.* 33 (2004) 748–749.
- [38] S.H. Park, S.H. Kang, I., Belharouak, Y.-K. Sun, K. Amine, *J. Power Sources* 177 (2008) 177–183.
- [39] D.-K. Lee, S.-H. Park, K. Amine, H.J. Bang, J. Parakash, Y.-K. Sun, *J. Power Sources* 162 (2006) 1346–1350.
- [40] Z. Lu, L.Y. Beaulieu, R.A. Donaberger, C.L. Thomas, J.R. Dahn, *J. Electrochim. Soc.* 149 (2002) A778–A791.
- [41] Z. Lu, J.R. Dahn, *J. Electrochim. Soc.* 150 (2003) A1044–A1051.
- [42] C.S. Johnson, N. Li, C. Lefief, J.T. Vaughey, M.M. Thackeray, *Chem. Mater.* 20 (2008) 6095–6106.
- [43] H. Deng, I. Belharouak, Y.-K. Sun, K. Amine, *J. Mater. Chem.* 19 (2009) 4510–4516.
- [44] M.-H. Lee, Y.-J. Kang, S.-T. Myung, Y.-K. Sun, *Electrochim. Acta* 50 (2004) 939–948.
- [45] A.S. Ito, D.C. Li, Y.C. Sato, M.M. Arao, M.B. Watanabe, M.H. Hatano, H.K. Horie, Y.K. Ohsawa, *J. Power Sources* 195 (2010) 567–573.
- [46] C.S. Johnson, J.S. Kim, C. Lefief, N. Li, J.T. Vaughey, M.M. Thackeray, *Electrochim. Commun.* 6 (2004) 1085–1091.
- [47] T.A. Arunkumar, E. Alvarez, A. Manthiram, *J. Electrochim. Soc.* 154 (2007) A770–A775.
- [48] X.-J. Guo, Y.-X. Li, M. Zheng, J.-M. Zheng, J. Li, Z.-L. Gong, Y. Yang, *J. Power Sources* 184 (2008) 414–419.
- [49] G.-Y. Kima, S.-B. Yi, Y.J. Park, H.-G. Kim, *Mater. Res. Bull.* 43 (2008) 3543–3552.
- [50] P. Kalyani, S. Chitra, T. Mohan, S. Gopukumar, *J. Power Sources* 80 (1999) 103–106.
- [51] S.-H. Kang, C.S. Johnson, J.T. Vaughey, K. Amine, M.M. Thackeray, *J. Electrochim. Soc.* 153 (2006) A1186–A1192.
- [52] J.-M. Kim, N.K. Kumagai, S.C. Komaba, *Electrochim. Acta* 52 (2006) 1483–1490.
- [53] R. Santhanam, P. Jones, A. Sumana, B. Rambabu, *J. Power Sources* 195 (2010) 7391–7396.